Confined Crystallization of Organic Materials in Nanopipettes: Tracking the Early Stages of Crystal Growth and Making Seeds for Unusual Polymorphs

Faduma M. Maddar, [a] *David Perry* [a] *and Patrick R. Unwin* [a,]*

[a] Department of Chemistry, University of Warwick, Coventry, CV4 7AL, UK

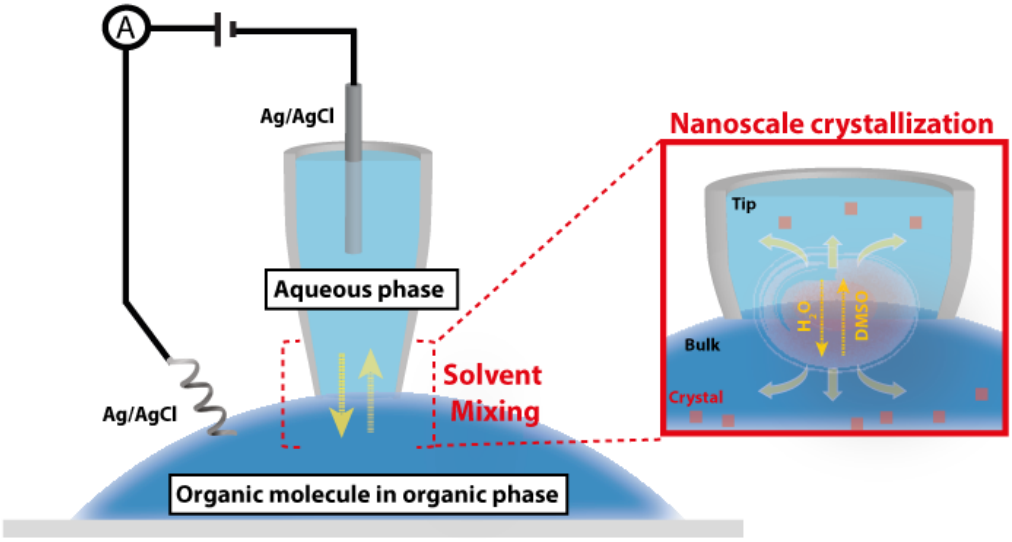

Table of Contents Graphic

ABSTRACT

Monitoring crystallization in real time at the nanoscale can provide valuable new insights into the nucleation process. Herein, the application of nanopipettes as nanoreactors to study the nucleation of organic materials (pharmaceutical crystals) is demonstrated, using bicalutamide (BIC), an active pharmaceutical ingredient of the prostate cancer drug CASODEX®, as a model. Crystallization is achieved using a nanoscale antisolvent system, whereby a nanopipette containing an aqueous inert salt solution is brought into contact with a dimethyl sulfoxide (DSMO) solution containing soluble BIC and the same inert salt (at the same concentration). Crystallization is driven and controlled by a combination of the applied bias between an electrode in the nanopipette and one in the bulk DMSO phase and mixing of the two solvents at the mouth of the nanopipette. Crystallization at the tip of the nanopipette causes transient blockages, as BIC particles form and translocate at the end of the nanopipette opening. At low inert electrolyte concentration, the current-time signature is highly stochastic and comprises a sequence of current pulse increases and decreases, which could either indicate nucleation-dissolution during phase transformation, and/or be due to the particles formed being charged. Particles produced in this way can be used as seeds for crystal growth and Raman spectroscopy analysis of the crystals produced indicates the formation of Form II BIC which is rarely formed. Thus, in addition to monitoring nucleation, nanopipettes can serve as reactors to synthesize organic crystals with polymorphs that are not typically found. Finite element method modeling provides valuable insight on the solvent mixing process and effect of applied bias, and helps to explain some of the observations.

INTRODUCTION

Crystallization at the nanoscale, in a confined environment, can have a significant impact on the properties of the emerging crystal structure, including the formation of unusual metastable polymorphs.[1] Herein, we show that nanopipettes provide a powerful methodology for detecting the nucleation and growth of seeds of pharmaceutical crystals, using bicalutamide (BIC) (shown in scheme 1), as an exemplar system. BIC is an active pharmaceutical ingredient (API) in AstraZeneca's prostate cancer product CASODEX®, belonging to class II of the biopharmaceutics classification system (BCS) (low solubility and high permeability).[2, 3] It has received considerable attention as a model for class II drugs.[4-6] Crystal polymorph control is an important aspect of drug formulation, to ensure bioavailability and stability of the drug product. Unusual polymorphs may provide a route to enhancing solubility of class II biopharmaceutics,[1, 7] and an aspect of this paper is the creation of polymorph II of BIC rather than the more stable polymorph I that is usually formed.

Nanopipettes and solid state nanopores, have become established as powerful tools in the detection and manipulation of single entities (nanoparticles and macromolecules) through the use of resistive pulse principles.[8-15] As an entity translocates through a pore connecting two electrolytic solutions (for example between the inside and outside of a nanopipette), with an applied bias, resulting changes in the ionic current can provide information about the size and surface properties of the entity, as well as its speed of translocation.[11, 16-20] Typically, the presence of an insulating particle in the orifice of a pore causes a transient increase in the pore resistance (decrease in the ionic current), [10, 17, 21, 22] the magnitude of which informs on the particle size.

Nanopipettes, are particularly attractive for resistive pulse experiments, as they can be prepared easily and rapidly from quartz or glass capillaries to give a range of tuned orifice

sizes, usually of conical geometry, simply by adjusting the laser puller parameters.[22-26] The conical shape of the nanopore has potential benefits in that the electric field is greatest at the opening, where the nanopipette becomes narrower, providing a higher sensitivity for resistive pulse sensing.[25] Consequently, applications of nanopipettes are expanding apace.[27-29] Of relevance to the studies herein, the use of nanopipettes as reaction centers for monitoring the nanoscale crystallization of zinc phosphate has been described.[30] While applying a voltage bias across the nanopipette opening, current oscillations were observed that were attributed to the precipitation and dissolution of zinc phosphate in the nanopipette opening. With precursor zinc and phosphate salts, one in the nanopipette and the other in the bathing solution, it was demonstrated that the sign of the applied bias could be used to drive either crystallization or dissolution at the nanopipette opening. We recently used this methodology to monitor the crystallization and dissolution of calcium carbonate in nanopipettes and showed this to be a powerful platform for rapidly screening crystal growth additives.[31] Additionally, the formation of inorganic salt nanoparticles in conical nanopores has been reported.[32-34]

The above examples have considered aqueous crystallization, but some work in much larger pores, in borosilicate glass or silicon nitride, have considered the use of different solvents either side of the pore mouth (solvent/antisolvent system), which mix at the pore to produce a supersaturated solution.[35] This is the type of system considered herein, but with the use of much smaller pores (50 nm diameter) formed using glass nanopipettes. Studies on this dimension are especially interesting because unusual polymorphs might be expected, due to the dramatic size-dependent stability properties of polymorphs on this length scale.[36] With the use of finite element method (FEM) modeling, we provide insight into the solvent mixing phenomenon that leads to precipitation and the strong effect of applied bias that we see. These new studies suggest that nanopipettes are potentially very useful devices for monitoring the nucleation of crystals in an antisolvent system and creating seeds for unusual polymorphs.

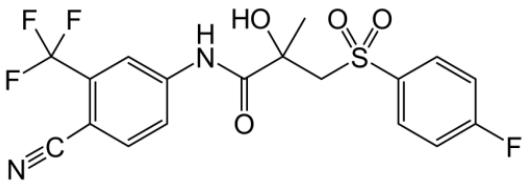

Scheme 1. Molecular structure of BIC.

EXPERIMENTAL

Solutions

For all experiments, unless stated otherwise, the nanopipette contained 100 mM tetrabutyl ammonium chloride (TBA^+Cl^-), from Sigma-Aldrich, in ultrapure water (Purite, Select HP) of resistivity 18.2 MΩ cm (at 25 ºC). The bath solution consisted of dimethyl sulfoxide (DMSO, Fisher, purity 99.7%) solution containing 100 mM TBA^+Cl^- and 5 mM BIC. Solid crystalline BIC was kindly supplied by AstraZeneca.

Nanopipettes

Nanopipettes were fabricated from quartz capillaries, with an outer diameter of 1.00 mm and an inner diameter of 0.5 mm (Friedrich and Dimmock). Using a laser puller (P-2000, Sutter instruments), capillaries were pulled to give a nanopipette with an opening diameter of approximately 50 nm at the end and semi-angle that over a few microns from the end approximated to *ca.* 3.7˚. Several pulled pipettes were examined by transmission electron microscope (TEM) to confirm these dimensions were consistent.[26, 37, 38]

BIC Crystallization Measurements

A two-electrode setup was employed with a AgCl-coated Ag quasi-reference counter electrode (QRCE) inserted into a nanopipette filled with aqueous TBACl solution and a second similar QRCE was placed in the bulk DMSO solution. The current, *I*, was measured as a function of time with the potential, *V*, applied in a defined way (constant or linearly scanned with time), using a home-built potentiostat and electrometer. Potential control and data acquisition was achieved using an field-programmable gate array (FPGA) card (7852R, National Instruments) controlled by a LabVIEW 2013 interface, National Instruments. All measurements were made at 23 ± 1 °C. The potential of Ag/AgCl electrode in DMSO was monitored over time and was

found to be stable (Supporting Information, section SI-3). The AgCl-coated Ag wire functions as a stable electrode in many aqueous media.[31, 39-42]

Raman Spectroscopy

Raman microscopy investigations of individual crystals employed a Renishaw inVia Reflex Raman Microscope fitted with a Charge Coupled Device (CCD) detector with a near-IR (633 nm) laser. A 50× objective lens was used.

Finite Element Method Simulations

Finite element method (FEM) simulations were carried out to understand the mixing zone of the two solvents and extract saturation levels of BIC near the mouth of the nanopipette. These simulations were done using COMSOL Multiphysics 5.2a using the transport of diluted species and electrostatics modules. Simulations used a 2D axisymmetric cylindrical geometry. The simulation domain, diffusion coefficients and boundary conditions are presented in Supporting Information, section SI-4. Briefly, mixing of the solvents was treated as a diffusive process, given the nanoscale dimensions of the system[43], with bulk concentration of 55 M water initially inside the pipette and 14.1 M DMSO in the bulk solution. The simulations accounted for the dependence of the diffusion coefficient of H_2O and DMSO on the H_2O: DMSO ratio (Supporting Information, section SI-5, Table S1), but for simplicity assumed no changes in the solution density (volume) in the mixing zone, so that a Newtonian fluid model could be assumed (Supporting Information, section SI-6). 100 mM TBA^+Cl^- was present inside and outside the pipette, with 5 mM BIC in the bath solution. Simulations considered several different applied biases, of relevance to the experiments. Saturation levels of BIC at different spatial locations were calculated based on the local proportion of water to DMSO, and measured saturation levels (Supporting Information, section SI-7).

RESULTS AND DISCUSSION

Crystallization of Bicalutamide in a Nanopipette

A schematic of the typical experimental setup for monitoring BIC nucleation and growth events is depicted in Figure 1. As mentioned above, the nanopipette was filled with 100 mM TBA^+Cl^- dissolved in water, and this was placed in a bath consisting of 5 mM BIC and 100 mM TBA^+Cl^- dissolved in DMSO. Note that for many of the experiments the concentration of BIC used (5 mM) was much lower than the saturation concentration in pure DMSO (200 mM), but occasionally different concentrations were used, as stipulated herein. A bias applied between the QRCE in the nanopipette and one in bulk solution generated an ionic current that could be used to monitor changes in the resistance at the end of the nanopipette. When a bias of -0.3 V was applied to the nanopipette electrode, transient current blockages (current decreases) were observed in the current-time (*I-t*) trace, as shown in Figure 2 (a) (i). These events, which have a frequency of 0.8 ± 1 min^{-1} (data provided in Supporting information, section SI-8), are attributed to the formation of BIC crystals near the end of the nanopipette, causing an increase in the system resistance and decrease in the ionic current. A zoom view of one of the events (Figure 2 (a) (ii)) shows that they are relatively slow (*ca.* 100 ms), with a very sharp decrease in current, followed by a slower recovery to the nanopipette open state current. Experiments performed with different biases revealed that these events exhibited a dependence on the applied bias. Figure 2 (b) and (c) show samples from *I-t* traces performed with applied bias of -0.1 V and -0.5 V. With increasing bias, a higher frequency of blockage events was observed.

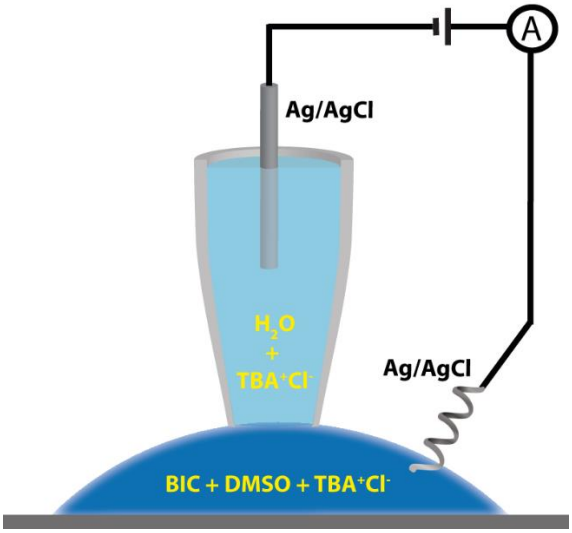

Figure 1. Setup (not to scale) for voltage dependent nucleation of BIC in conical nanopipettes. A bias was applied between an electrode in a nanopipette containing aqueous electrolyte and an electrode in DMSO solution containing BIC. The current response was measured as a function of time and applied potential.

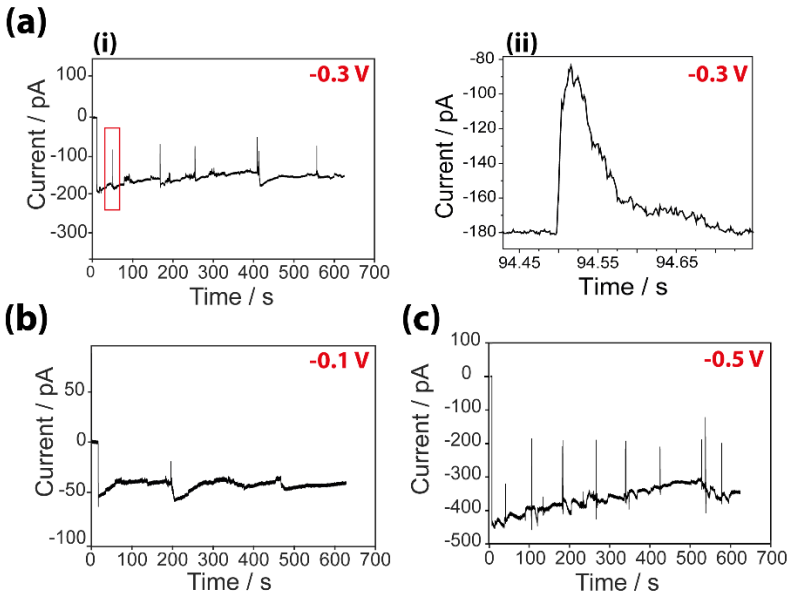

Figure 2. Current-time response with 5 mM BIC in the DMSO bath at different potentials applied to the tip with respect to the Ag/AgCl electrode in bulk: (a) (i) -0.3 V, with inset (ii) showing expanded view of highlighted event; (b) -0.1 V; and (c) -0.5 V.

To confirm that the blockage events were due to BIC, the *I-t* and current-voltage (*I-V*) behavior were also recorded in cases where 0 mM and 200 mM BIC was present in the bath DMSO solution. Figure 3 (a) (i) shows example *I-t* data for a tip bias of -0.3 V for the case where no BIC was present in the bath solution. Under these conditions, a featureless, steady *I-t* trace was observed, with no transient blockages, suggesting that the nanopipette remained in its open state throughout. The open state current is *ca.* -150 pA, broadly similar to the open state in Figure 2 (a) (i), recorded with a different nanopipette. Likewise, the *I-V* curve in Figure 3 (a) (ii) shows the rectification characteristics expected for a small tip of this size,[44] that have negatively charged walls.[45-47]

With the same nanopipette electrode bias of -0.3 V, but higher concentration of 200 mM BIC in the DMSO phase (Figure 3 (b) (i)), a very high frequency of blockages was observed, manifested as an oscillating current between the open and blocked state. In fact, the frequency of events is so high that a fully open state current is never achieved. At 10 mM and 20 mM BIC in the DMSO solution the event frequency was 4.1 ± 2 and 8.2 ± 4 min^{-1}, respectively (data provided in Supporting information, section SI-8). These data indicate that the frequency of events is strongly dependent on BIC concentration in the DMSO phase.

The *I-V* measurements presented in Figure 3 (b) (ii) further reveals the effect of applied bias on the blockage behavior. At negative tip potentials with 200 mM BIC in DMSO, rapid blockage and clearance events to an open state are observed, but such behavior is not seen at positive tip potentials or in the case where no BIC is present (Figure 3 (a) (ii)).

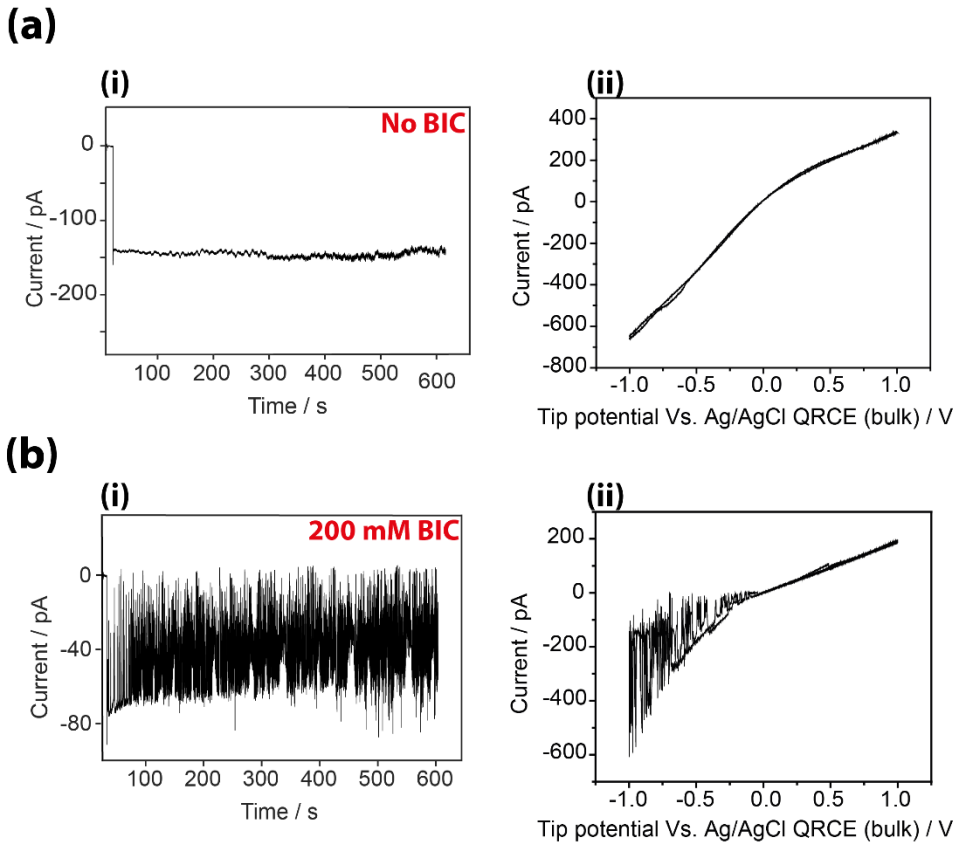

Figure 3. Current-time response at a nanopipette electrode potential of -0.3 V for: (a) (i) no BIC in DMSO and (b) (i) 200 mM BIC in DMSO. Corresponding *I-V* curves of each nanopipette prior to current-time measurements are shown in (a) (ii) and (b) (ii).

Nanoprecipitation events observed herein are driven predominantly by the antisolvent effect[48] due to the poor solubility of BIC in water (11.6 μM).[4] Based on our experimental observations, we propose that the DMSO and water phases mix locally and rapidly (*vide infra*) at the nanopipette opening. This mixing leads to the protonation of BIC by water, as BIC has a pKa of 12,[5] as illustrated in Figure 4. Consequently, at negative nanopipette electrode biases, protonated BIC (positively charged) will be driven into the body of the nanopipette by the applied electric field, but the high-water content of the mixed phase at the end of the nanopipette (*vide infra*), means that the solution becomes locally supersaturated with respect to BIC and nucleation occurs. Particle formation (and growth) causes a transient increase in

the system resistance and blockage of the ionic current. In contrast, in the case where a positive tip bias was applied, no blockage events were seen, consistent with protonated BIC being largely excluded from the nanopipette opening. Thus, the applied bias has a significant effect in promoting or inhibiting crystallization, even though the two solvents presumably mix to similar extents irrespective of the bias.

The blip responses observed, suggest a process where BIC particles form (leading to a decrease in the ion conductance current) and subsequently either translocate out of the pipette orifice or move further up the conical pipette whose dimensions get wider, re-establishing the baseline open-state conductance current. It has previously been shown that the surface charge of a translocating particle can have an impact on the shape of the resistive pulse and is strongly influenced by the concentration of supporting electrolyte used.[11, 49, 50] High electrolyte concentration screens the charge on the particle and the nanopipette walls (short Debye length) and so particle charge has little effect, whereas at low electrolyte concentration the Debye length is larger. To explore this aspect, *I-t* measurements were performed with a lower electrolyte concentration (10 mM TBA^+Cl^-), with some example data shown in Figure 5. In these instances, the transient shape is more complicated showing both an increase resistive pulse, described above, but accompanied by an increase in conductance state at some times in an overall "event". These features are broadly similar to features seen on charged particles[49-53] although in the case of Figure 5, the features are much more complex and could also result from some repetitive nucleation and redissolution events in the growth of a particle (e.g. transformation from one solid phase to another via a solution-mediated process). Additionally, these events are somewhat slow for a particle translocation event,[49] and would suggest that the particle, and evolving entity, rattles in the end of the pipette before leaving the reaction zone. Based on the fact that BIC is protonated in the aqueous phase, the surface charge of the particle is likely to be positive. In this case, the particle would be expected to migrate into the

nanopipette (given the applied field) but, as we show below, some particles evidently leave the nanopipette, perhaps due to physical flow of the more dense aqueous phase into the DMSO phase, which is not considered in the simplified model we present below.

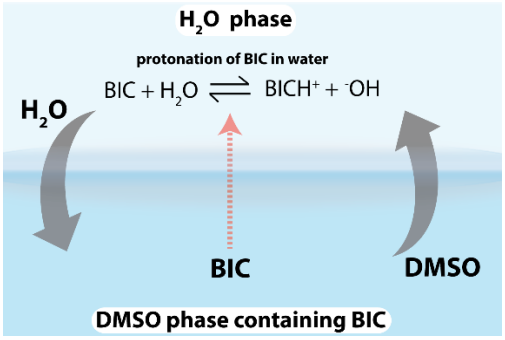

Figure 4. Water-DMSO mixing near the mouth of the nanopipette and the subsequent transfer and protonation of BIC in the water phase.

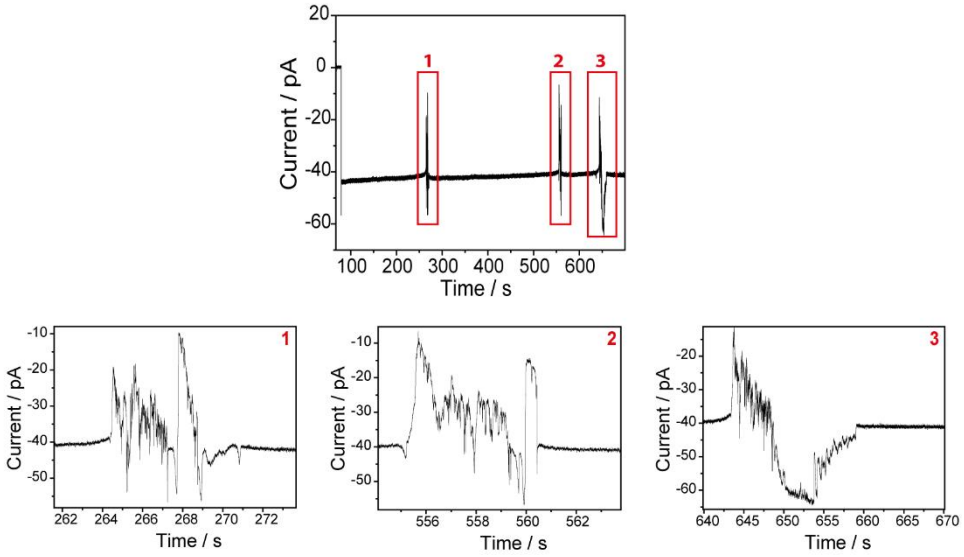

Figure 5. Current-time response at a nanopipette electrode potential of -0.3 V using 10 mM TBA^+Cl^- in each phase and 5 mM BIC in the DMSO phase. Expanded views of highlighted events (1-3) are shown.

In order to estimate saturation levels of BIC inside a nanopipette, time-dependent FEM simulations were performed with 100 mM TBA^+Cl^- in the nanopipette (water) and bath DMSO

solutions. 5 mM BIC was present in the bath solution at the start of the simulation. BIC had neutral charge in the bulk organic phase and became protonated in the aqueous phase, as shown in Figure 4, and further discussed in the Supporting Information, section SI-4.

Figure 6 presents profiles that show of how the concentrations of water and DMSO in the end of the nanopipette, as well as the local saturation level of BIC, varies with time after immersing a nanopipette (aqueous solution) into a bath (DMSO). A bias of -0.3 V was applied to the nanopipette electrode. It can be seen that the water concentration towards the end of the pipette decreases from the bulk value, as water is transported out of the nanopipette into the DMSO phase. The DMSO concentration, on the other hand, can be seen to propagate up the length of the pipette with increasing time as DMSO diffuses into the pipette. The diffusion of BIC into the nanopipette, together with the higher concentration of water, results in the solution becoming highly supersaturated with respect to BIC, with extreme saturation levels ($\Omega = [BIC]_{total} / [BIC]_{sat}$) of up 140, which is the reason why the crystallization process is so driven. It can be seen that quasi-steady profiles are produced at times between 10 ms and 100 ms.

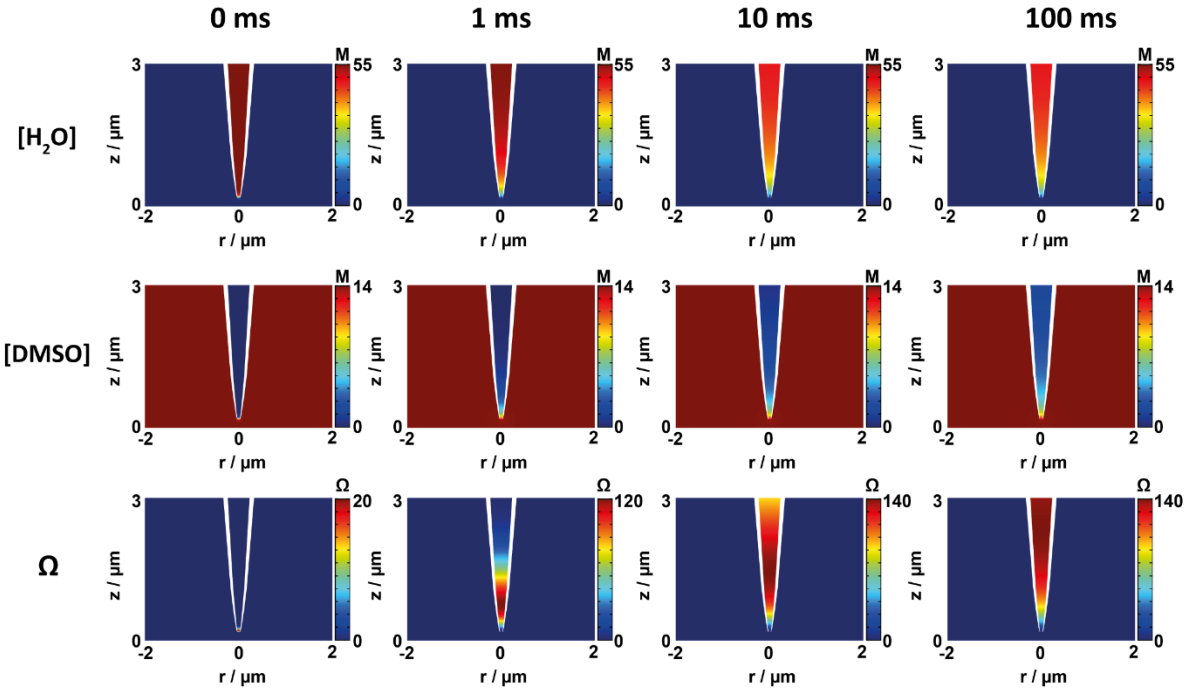

Figure 6. FEM simulations showing concentration profiles of water, DMSO and BIC saturation levels ($\Omega = [BIC]_{total} / [BIC]_{sat}$) at times of 0 ms, 1 ms, 10 ms and 100 ms after immersing a nanopipette containing aqueous electrolyte into DMSO (5 mM BIC and electrolyte). Nanopipette electrode bias of -0.3 V.

The experimental data presented and discussed above, suggest a strong influence of the applied bias polarity on the crystallization process. Crystallization was only seen in the case where a negative bias was applied to the nanopipette electrode. This behavior was explored further with FEM simulations. After a diffusional mixing time of 1 second, with an applied bias of -0.3 V to the nanopipette electrode, high relative saturation levels were observed throughout the tip, of up to $\Omega = 142$ were observed a few microns up the length of the nanopipette (Figure 7 (a)). At these high saturation levels, nucleation and growth of BIC crystals is strongly favored, as mentioned above. In contrast, in the case where a positive bias was applied, Ω values above 1 were not seen, as shown in Figure 7 (b) and so crystallization would not be expected, as is the case experimentally under these conditions. Importantly, the solution was never supersaturated ($\Omega > 1$) outside of the nanopipette domain, in either case, suggesting that any BIC particles must form inside the pipette.

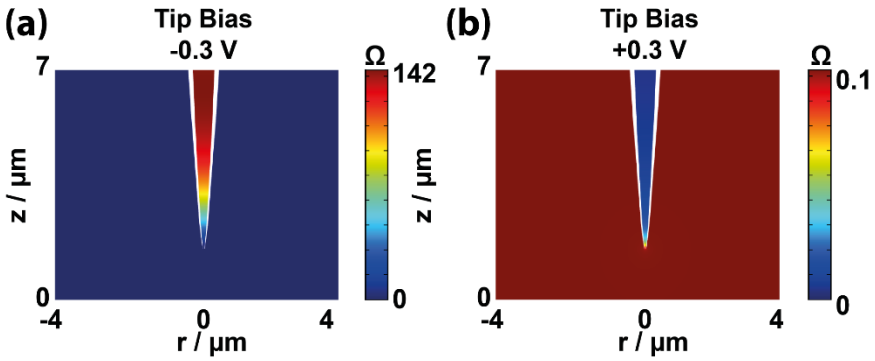

Figure 7. Predicted BIC saturation levels with a bias of -0.3 V (a) and +0.3 V (b) applied to the upper nanopipette boundary. FEM Simulations were performed in 100 mM TBA^+Cl^- with 5 mM BIC in the DMSO phase initially.

To accelerate the process, Figure 8 (a) shows an optical micrograph taken of a nanopipette after BIC growth experiments had been performed for ~10 min with 200 mM BIC in the bath. It reveals solid products formed from these experiments inside the tip. Crystals were also found to grow on the glass surface directly beneath where the probe was positioned for these growth experiments (Figure 8 (b)). The presence of these crystals outside the nanopipette is evidence that particles translocate the nanopipette orifice, and continue to grow and settle on the glass substrate beneath. Crystals were not observed in cases where a positive tip bias was applied to the electrode in the nanopipette.

To confirm that the crystals formed were BIC, Raman Spectroscopy was employed, shown in Figure 8 (c). Characterization of the resulting peaks for these samples lead to the conclusion that the formed crystals are of Form II BIC (comparing the data to Raman spectroscopy of reference compounds elsewhere).[54] In particular, the strong peak at around 1600 cm^{-1} is found in both BIC Forms, but the Form II crystal has π-π stacking interactions, which causes an extra peak at 1582 cm^{-1}, as highlighted in Figure 8 (c) that is not present in the spectrum of Form I. Form I is the more stable polymorph at all temperatures and Form II is labelled as the metastable state.[55] Crystallization of BIC from bulk solutions at room temperature usually leads to Form I. Form II can be produced from the transformation of (solid-state) amorphous BIC at room temperature and this could be the route followed in this case, i.e. the high supersaturations that are attained at the end of the nanopipette (Figure 7 (a)) could promote crystallization of the amorphous form, with transition to Form II.[55] A further consideration is that at the nanoscale, smaller crystals generally have higher free energies than larger ones, and the formation of the polymorph with the thermodynamically most stable bulk structure is not necessarily the one with the most stable surface structure.[56-58] Crystal surface energy is significant for polymorph stability and the effect is further emphasized when the nature of the solvent is considered.[36, 56]

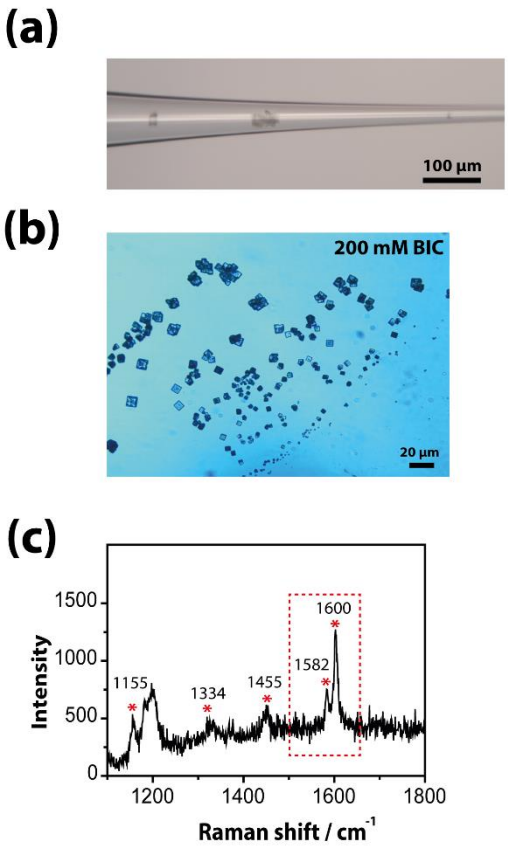

Figure 8. (a) Optical image of a typical nanopipette used in time-current measurements with 200 mM BIC in bath showing the formation of crystals inside the tip. (b) Additional formation of crystals in the bath containing 200 mM BIC after a nanopipette crystallization experiment. (c) Raman spectrum of BIC crystals formed, with main peak positions marked. The peaks highlighted at 1582 and 1600 cm^{-1} are most useful in resolving the BIC crystal type.

CONCLUSION

In this study, we have shown that the nucleation and growth of BIC nanoparticles can be induced and monitored in real time using a simple nanopipette system. The approach advocated is an antisolvent/solvent approach in which crystallization is induced by the mixing of DMSO and water at the mouth of a nanopipette, with the applied bias providing control over the extent of crystallization. The bias applied can be used to promote or stop nucleation. Simultaneously, by measuring the current-time response at a given applied potentials current oscillations are observed which were attributed to, and shown to result from, the formation, and subsequent translocation, of BIC particles near the nanopipette orifice.

With this simple approach, we have demonstrated that seeds can be produced that lead to the formation of Form II BIC at room temperature. To support the experiments, detailed FEM simulations have provided valuable information that help to validate the nucleation process, and provide estimates for the supersaturation levels achieved experimentally. In the future, with this unique, simple yet powerful nanoscale methodology, other APIs with polymorphic properties could be explored, as well as formulations of amorphous solid dispersions. There is also, the possibility of implementing this system for seed synthesis at larger scales, using multi porous membranes and designer potential-time profiles that promote nucleation and particle ejection.

AUTHOR INFORMATION

Corresponding Author

* E-mail: p.r.unwin@warwick.ac.uk.

ACKNOWLEDGEMENTS

We thank Dr Leslie Hughes and Dr Stephen Wren of AstraZeneca for providing us with the bicalutamide sample and funding. We thank the EPSRC MOAC grant for funding for F.M.M., the Leverhulme Trust *via* a research project grant for funding D.P. and the Royal Society for a Wolfson Research Merit Award for P.R.U.

SUPPORTING INFROMATION

The SI includes: Data on the potential of an Ag/AgCl electrode in DMSO over time; FEM model details and a schematic; diffusion coefficients of H_2O and DMSO for different compositions used in simulations; a brief note on densities and molar volumes of H_2O and DMSO at different ratios; and UV-Vis spectra of bicalutamide dissolved in different ratios of H_2O and DMSO, with acquired saturation concentrations.

REFERENCES

(1) Vippagunta, S. R.; Brittain, H. G.; Grant, D. J. W. *Adv. Drug Deliv.Rev.* **2001**, 48, 3-26.

(2) Abu-Diak, O. A.; Jones, D. S.; Andrews, G. P. *J. Pharm. Sci.* **2012**, 101, 200-213.

(3) Andrews, G. P.; AbuDiak, O. A.; Jones, D. S. *J. Pharm. Sci.* 99, 1322-1335.

(4) Ren, F.; Jing, Q.; Tang, Y.; Shen, Y.; Chen, J.; Gao, F.; Cui, J. *Drug Dev. Ind. Pharm.* **2006**, 32, 967-972.

(5) Kumbhar, D. D.; Pokharkar, V. B. *Colloids Surf. A* **2013**, 416, 32-42.

(6) Li, C.; Li, C.; Le, Y.; Chen, J.-F. *Int. J. Pharm.* **2011**, 404, 257-263.

(7) Singhal, D.; Curatolo, W. *Adv. Drug Deliv. Rev.* **2004**, 56, 335-347.

(8) DeBlois, R. W.; Bean, C. P. *Rev. Sci. Instrum.* **1970**, 41, 909-916.

(9) Kozak, D.; Anderson, W.; Vogel, R.; Trau, M. *Nano today* **2011**, 6, 531-545.

(10) Berge, L. I.; Feder, J.; Jo/ssang, T. *Rev. Sci. Instrum.* **1989**, 60, 2756-2763.

(11) Holden, D. A.; Hendrickson, G.; Lyon, L. A.; White, H. S. *J. Phys. Chem. C* **2011**, 115, 2999-3004.

(12) Keyser, U. F. *J. R. Soc. Interface* **2011**, 8, 1369-1378.

(13) Venkatesan, B. M.; Bashir, R. *Nat. Nanotechnol.* **2011**, 6, 615-624.

(14) Heins, E. A.; Siwy, Z. S.; Baker, L. A.; Martin, C. R. *Nano Lett.* **2005**, 5, 1824-1829.

(15) Shi, W.; Friedman, A. K.; Baker, L. A. *Anal. Chem.* **2017**, 89, 157-188.

(16) Fraccari, R. L.; Ciccarella, P.; Bahrami, A.; Carminati, M.; Ferrari, G.; Albrecht, T. *Nanoscale* **2016**, 8, 7604-7611.

(17) Bayley, H.; Martin, C. R. *Chem. Rev.* **2000**, 100, 2575-2594.

(18) Ying, Y.-L.; Long, Y.-T. *Sci. China Chem.* **2017**, 60, 1187-1190.

(19) Gao, R.; Lin, Y.; Ying, Y.-L.; Liu, X.-Y.; Shi, X.; Hu, Y.-X.; Long, Y.-T.; Tian, H. *Small* **2017**, 13, 1700234

(20) Gao, R.; Ying, Y.-L.; Hu, Y.-X.; Li, Y.-J.; Long, Y.-T. *Anal. Chem.* **2017**, 89, 7382-7387.

(21) DeBlois, R. W.; Bean, C. P.; Wesley, R. K. A. *J. Colloid Interface Sci.* **1977**, 61, 323-335.

(22) Howorka, S.; Siwy, Z. *Chem. Soc. Rev.* **2009**, 38, 2360-2384.

(23) Murray, R. W. *Chem. Rev.* **2008**, 108, 2688-2720.

(24) Dekker, C. *Nat. Nanotechnol.* **2007**, 2, 209-215.

(25) Lan, W.-J.; Holden, D. A.; Zhang, B.; White, H. S. *Anal. Chem.* **2011**, 83, 3840-3847.

(26) Perry, D.; Momotenko, D.; Lazenby, R. A.; Kang, M.; Unwin, P. R. *Anal. Chem.* **2016**, 88, 5523-5530.

(27) Vilozny, B.; Actis, P.; Seger, R. A.; Vallmajo-Martin, Q.; Pourmand, N. *Anal. Chem.* **2011**, 83, 6121-6126.

(28) Cai, H.; Wang, Y.; Yu, Y.; Mirkin, M. V.; Bhakta, S.; Bishop, G. W.; Joshi, A. A.; Rusling, J. F. *Anal. Chem.* **2015**, 87, 6403-6410.

(29) Morris, C. A.; Friedman, A. K.; Baker, L. A. *Analyst* **2010**, 135, 2190-2202.

(30) Vilozny, B.; Actis, P.; Seger, R. A.; Pourmand, N. *ACS Nano* **2011**, 5, 3191-3197.

(31) Perry, D.; Parker, A. S.; Page, A.; Unwin, P. R. *ChemElectroChem* **2016**, 3, 2212-2220.

(32) Siwy, Z. S.; Powell, M. R.; Petrov, A.; Kalman, E.; Trautmann, C.; Eisenberg, R. S. *Nano Lett.* **2006**, 6, 1729-1734.

(33) Powell, M. R.; Sullivan, M.; Vlassiouk, I.; Constantin, D.; Sudre, O.; Martens, C. C.; Eisenberg, R. S.; Siwy, Z. S. *Nat. Nanotechnol.* **2008**, 3, 51-57.

(34) Innes, L.; Powell, M. R.; Vlassiouk, I.; Martens, C.; Siwy, Z. S. *J. Phys. Chem. C* **2010**, 114, 8126-8134.

(35) Yusko, E. C.; Billeh, Y. N.; Mayer, M. *J. Phys.: Condens. Matter* **2010**, 22, 454127.

(36) Belenguer, A. M.; Lampronti, G. I.; Cruz-Cabeza, A. J.; Hunter, C. A.; Sanders, J. K. M. *Chem. Sci.* **2016**, 7, 6617-6627.

(37) Sa, N.; Baker, L. A. *J. Electrochem. Soc.* **2013**, 160, H376-H381.

(38) Chen, C.-C.; Baker, L. A. *Analyst* **2011**, 136, 90-97.

(39) Ebejer, N.; Güell, A. G.; Lai, S. C.; McKelvey, K.; Snowden, M. E.; Unwin, P. R. *Annu. Rev. Anal. Chem.* **2013**, 6, 329-351.

(40) Patel, A. N.; Collignon, M. G.; O'Connell, M. A.; Hung, W. O. Y.; McKelvey, K.; Macpherson, J. V.; Unwin, P. R. *J. Am. Chem. Soc.* **2012**, 134, 20117-20130.

(41) Maddar, F. M.; Lazenby, R. A.; Patel, A. N.; Unwin, P. R. *Phys. Chem. Chem. Phys.* **2016**, 18, 26404-26411.

(42) Güell, A. G.; Meadows, K. E.; Dudin, P. V.; Ebejer, N.; Macpherson, J. V.; Unwin, P. R. *Nano Lett.* **2014**, 14, 220-224.

(43) Lee, C.-Y.; Chang, C.-L.; Wang, Y.-N.; Fu, L.-M. *Int. J. Mol. Sci.* **2011**, 12, 3263-3287.

(44) Wei, C.; Bard, A. J.; Feldberg, S. W. *Anal. Chem.* **1997**, 69, 4627-4633.

(45) White, H. S.; Bund, A. *Langmuir* **2008**, 24, 2212-2218.

(46) Momotenko, D.; Girault, H. H. *J. Am. Chem. Soc.* **2011**, 133, 14496-14499.

(47) Lan, W.-J.; Edwards, M. A.; Luo, L.; Perera, R. T.; Wu, X.; Martin, C. R.; White, H. S. *Acc. Chem. Res.* **2016**, 49, 2605-2613.

(48) Lonare, A. A.; Patel, S. R. *Int. J. Chem. Eng. Appl.* **2013**, 4, 337.

(49) Lan, W.-J.; Kubeil, C.; Xiong, J.-W.; Bund, A.; White, H. S. *J. Phys. Chem. C* **2014**, 118, 2726-2734.

(50) Menestrina, J.; Yang, C.; Schiel, M.; Vlassiouk, I.; Siwy, Z. S. *J. Phys. Chem. C* **2014**, 118, 2391-2398.

(51) Chang, H.; Kosari, F.; Andreadakis, G.; Alam, M. A.; Vasmatzis, G.; Bashir, R. *Nano Lett.* **2004**, 4, 1551-1556.

(52) Kowalczyk, S. W.; Dekker, C. *Nano Lett.* **2012**, 12, 4159-4163.

(53) Smeets, R. M. M.; Keyser, U. F.; Krapf, D.; Wu, M.-Y.; Dekker, N. H.; Dekker, C. *Nano Lett.* **2006**, 6, 89-95.

(54) Tres, F.; Patient, J. D.; Williams, P. M.; Treacher, K.; Booth, J.; Hughes, L. P.; Wren, S. A. C.; Aylott, J. W.; Burley, J. C. *Mol. Pharm.* **2015**, 12, 1512-1522.

(55) Vega, D. R.; Polla, G.; Martinez, A.; Mendioroz, E.; Reinoso, M. *Int. J. Pharm.* **2007**, 328, 112-118.

(56) Navrotsky, A.; Mazeina, L.; Majzlan, J. *Science* **2008**, 319, 1635-1638.

(57) McHale, J. M.; Navrotsky, A.; Perrotta, A. J. *J. Phys. Chem. B* **1997**, 101, 603-613.

(58) Navrotsky, A. *ChemPhysChem* **2011**, 12, 2207-2215.